Check for updates

Biomass-derived O, N-codoped hierarchically porous carbon prepared by black fungus and *Hericium erinaceus* for high performance supercapacitor†

Xinxian Zhong, [ID] [a] Quanyuan Mao,[a] Zesheng Li, [ID] [b] Zhigao Wu,[c] Yatao Xie,[d] Shu-Hui Li, [ID] *[a] Guichao Liang[a] and Hongqiang Wang [ID] *[a]

Biomass-derived carbon materials have been widely researched due to their advantages such as low cost, environmental friendliness, readily available raw materials. Black fungus and *Hericium erinaceus* contain many kinds of amino acids. In this paper, unique O, N-codoped black fungus-derived activated carbons (FAC_X), and *Hericium erinaceus*-derived activated carbons (HAC_X) were prepared by KOH chemical activation under different temperatures without adding additional reagents containing nitrogen and oxygen functional groups, respectively. As electrode materials of symmetric supercapacitors, FAC_2 and HAC_2 calcined at 800 °C exhibited the highest specific capacitance of 209.3 F g^{-1} and 238.6 F g^{-1} at 1.0 A g^{-1} in the two-electrode configuration with 6.0 M KOH as the electrolyte, respectively. The X-ray photoelectron spectroscopy confirmed that the as-synthesized FAC_X and HAC_X contained small amounts of nitrogen and oxygen elements. Moreover, heteroatom-doped FAC_2 and HAC_2 electrode materials shown excellent rate performance (84.1% and 75.0% capacitance retention at 20 A g^{-1}, respectively). By comparison, the oxygen-rich hierarchical porous carbon (HAC_2) shows higher specific capacitance and energy density and longer cycling performance. Nevertheless, carbon-rich hierarchical porous carbon (FAC_2) indicates excellent rate performance. Biomass-derived heteroatom self-doped porous carbons are expected to become ideal active materials for high performance supercapacitor.

Introduction

With the rapid development of modern society, the increasing demand for renewable energy has stimulated great interest in electrochemical energy conversion and storage.[1,2] Supercapacitors are also called electrochemical capacitors, and are widely recognized as promising energy storage systems because of their unique properties such as high power density, fast charge–discharge rate, outstanding cycling stability and environmental friendliness. These advantages of supercapacitors can make up the shortage of conventional capacitors and batteries in many application fields.[3,4] Meanwhile, the electrochemical performance of supercapacitors mainly depends on the electrode materials, and their physicochemical properties are a crucial and vital factor for supercapacitors. Therefore, searching for excellent electrode materials will greatly facilitate the future developments of supercapacitors.[5–8]

Carbon materials, conducting polymers[9] and metal oxides[10] as electrode materials of supercapacitors have been widely studied. Though conducting polymers and metal oxides have high theoretical specific capacitance due to their pseudocapacitance property, depending on the fast reversible redox reactions to storage energy,[11] the low conductivity and high cost are the main drawbacks of metal oxides, and the conducting polymers structure suffers repetitive swelling and shrinkage during the progress of charge–discharge, and results in the decrease of the capacity and cycle life.[12] However, carbon materials are the earliest and the most widely studied electrode materials of supercapacitors. According to the storage energy mechanism, carbon materials belong to electric double-layer capacitors (EDLC), whose storage energy depends on the ion absorption–desorption at the interface between the electrolyte and the electrode.[13,14] Although the low energy density and the low theoretical specific capacitance, these carbon-based materials including activated carbon, carbon nanotubes, graphene, carbon nanofiber, porous carbon and their derivatives exhibit excellent

[a] State Key Laboratory for the Chemistry and Molecular Engineering of Medicinal Resources, Guangxi Key Laboratory of Low Carbon Energy Materials, School of Chemistry and Pharmaceutical Sciences, Guangxi Normal University, Guilin, 541004, China. E-mail: gxnulsh@gxnu.edu.cn; whq74@mailbox.gxnu.edu.cn

[b] College of Chemistry, Guangdong University of Petrochemical Technology, Maoming, 525000, China

[c] Guangxi Vocational and Technical Institute of Industry, Nanning, 530005, China

[d] School of Materials Science and Engineering, Ocean University of China, Qingdao, 266100, China

† Electronic supplementary information (ESI) available. See DOI: 10.1039/d1ra03699h

performance such as good conductivity, high thermal stability, high specific surface area, meanwhile the low cost and abundant resources of carbon have attracted many researchers concentrating on new carbon materials.[15–19]

Biomass materials have been widely selected as precursors to fabricate porous carbon materials with different morphologies for supercapacitors.[20] These biomass materials include rapeseed dregs,[21] loofah sponge,[22] willow catkin,[23] shiitake mushroom,[24] potato starch,[25] bamboo char,[26] bacterial cellulose,[27] walnut shell,[28] tobacco rods,[29] corn grain,[30] rice husk,[31] osmanthus flower,[32] peanut shell,[33] sunflower seed shell,[34] corncob,[35] cornstalk,[36] *etc.* Most biomass-derived carbon materials as mentioned above possess an excellent electrochemical capacitive performance. Cheng *et al.* reported a hierarchically porous carbon (the specific surface area reaches up to 2988 m^2 g^{-1}) *via* H$_3$PO$_4$ carbonization and KOH activation from natural shiitake mushroom for supercapacitor, which exhibits a specific capacitance of 306 F g^{-1} at 1.0 A g^{-1} in three-electrode cell with 6.0 M KOH as electrolyte and delivers a specific capacitance of 238 F g^{-1} at 0.2 A g^{-1} in a two-electrode cell.[24] Zou *et al.* prepared a high-performance porous carbon (the specific surface area is 1463 m^2 g^{-1}) by KOH activation from osmanthus flower and applied it for supercapacitor, which displays the best specific capacitance of 255 F g^{-1} at 1.0 A g^{-1} in there-electrode cell using 6.0 M KOH as electrolyte.[32] Xu *et al.* improved an activated method of porous carbons derived from agricultural waste biomass corncobs *via* facile KOH solution soaking at room temperature prior to a one-step carbonization process.[35] The obtained porous carbon showed a high capacity of 394.9 F g^{-1} at a current density of 1.0 A g^{-1} in there-electrode system in a 6.0 M KOH aqueous electrolyte solution and the specific capacitance of the porous carbons-based supercapacitor measured under two-electrode configuration is 247 F g^{-1} at 0.5 A g^{-1}. Thus, hierarchical porous carbon can not only provide high specific surface area to store energy, but also shorten the diffusion distance of ions, which are beneficial to increasing the specific capacitance of supercapacitor.[37]

Furthermore, the electrochemical performance of porous carbon for supercapacitor usually could be improved by doping heteroatoms (*e.g.*, N, O and S atoms) in carbon framework. Especially, the oxygen and nitrogen functional groups can improve the surface wettability to promote the access of electrolyte and offer extra pseudocapacitance during charging and discharging process.[38–42] Therefore, developing a convenient method to prepare hierarchical porous carbon with suitable heteroatom functional groups is highly desirable for high performance supercapacitor.

Herein, we select black fungus and *Hericium erinaceus* containing rich protein and amino acid as resources of carbon to prepare oxygen and nitrogen codoped hierarchical porous carbon. In this work, black fungus-derived activated carbons (FAC$_X$) and *Hericium erinaceus*-derived activated carbons (HAC$_X$) were obtained by carbonization and KOH chemical activation under different temperature, respectively. The heteroatom-doped FAC$_2$ and HAC$_2$ calcined at 800 °C demonstrate porous 3D structure, moderate graphization degree and satisfied specific surface area, meanwhile FAC$_2$ and HAC$_2$ as electrode materials of supercapacitor exhibit excellent electrochemical performance.

Experimental

Fabrication of carbon materials

The preparation process schematic of FAC$_X$ and HAC$_X$ porous activated carbons is demonstrated in Fig. 1. Firstly, the black fungus and *Hericium erinaceus* bought from the market were ground by crushing mill, then were washed with distilled water and dried at 80 °C in vacuum oven, successively. Secondly, the desiccated black fungus and *Hericium erinaceus* powders were put into tube furnace and treated at 500 °C for 60 min under Ar atmosphere with a heating rate of 5 °C min^{-1}, respectively. The carbonized black fungus and *Hericium erinaceus* were washed with 1.0 M NaOH and 95% ethanol to remove metal ions and organic deposition within the products, respectively. The initial products were activated with KOH (KOH mixed with the initial product in a mass ratio of 3 : 1), then were calcined at 600 °C, 800 °C and 1000 °C with a heating rate of 2 °C min^{-1} under Ar atmosphere for 120 min, respectively. Finally, these obtained coarse products were washed with 1.0 M HCl and distilled water to remove excess KOH and dried in vacuum oven for 24 h. The as-obtained products were denoted as FAC$_X$ and HAC$_X$, where X = 1, 2 and 3 correspond to the temperature 600 °C, 800 °C and 1000 °C, respectively.

Electrochemical measurement

The fabrication procedure of electrode materials is as follows: carbon materials, polytetrafluoroethylene and carbon black were mixed together in a mass ratio of 8 : 1 : 1. Then they were dispersed into ethanol, stirred and heated into paste, later the paste was crushed about a thickness of 150 μm, the sheet was cut into electrodes with a diameter of 12 mm and then was dried under vacuum at 60 °C overnight. Then the symmetric button-type supercapacitor was assembled with polypropylene membrane as separator.

All the electrochemical tests were performed at the voltage range of 0–1.0 V in 6.0 M KOH aqueous solution at room temperature. The specific capacitance of two-electrode configuration was calculated based on the discharge curve according to the following formulas:
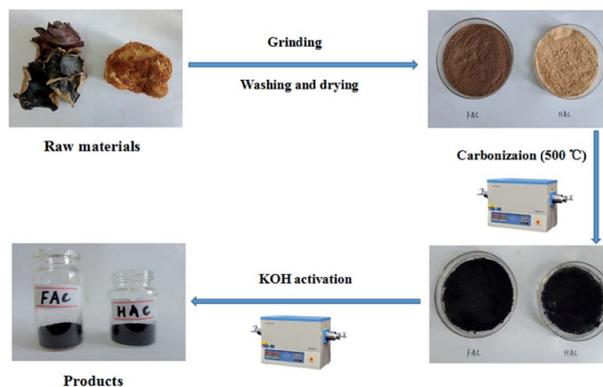
$$C = \frac{I\Delta t}{\Delta V} \tag{1}$$

Fig. 1 Preparation process schematic of FAC$_X$ and HAC$_X$.

$$\frac{1}{C} = \frac{1}{m_1 C_s} + \frac{1}{m_2 C_s} \tag{2}$$

where C and C_s represent the specific capacitance (F) and single electrode specific capacitance (F g^{-1}), respectively, I is the discharge current (A), Δt is the discharge time (s), ΔV corresponds to the potential window (V), m_1 and m_2 represent the mass (g) of active material on two electrodes.

The energy density and power density of supercapacitor were calculated according to the following formulas:

$$E = \frac{1}{8 \times 3.6} C_s V^2 \tag{3}$$

$$P = \frac{E}{\Delta t} \tag{4}$$

where E and P represent energy density (W h kg^{-1}) and power density (W kg^{-1}), respectively, C_s is the single electrode specific capacitance (F g^{-1}) of the supercapacitor, V is the voltage range (V), Δt is the discharge time (h).

Results and discussion

Materials characterization

The morphologies of FAC$_X$ and HAC$_X$ are demonstrated in Fig. 2. It is apparent that activation temperature has a great influence on morphology and pore size of as-prepared carbon materials. There are only some shallow pores on the surface of bulk and thick FAC$_1$ (shown in Fig. 2a) and HAC$_1$ (shown in Fig. 2d), which the initial products were activated at 600 °C. When the activation temperature increased to 800 °C, the as-obtained FAC$_2$ (shown in Fig. 2b) and HAC$_2$ (shown in Fig. 2e) emerge more pores, HAC$_2$ possesses more abundant pores with different sizes than FAC$_2$ and presents distinct three-dimensional network. From Fig. 2c and f, we can observe that more nano graphite sheets appear with the further increase of activation temperature to 1000 °C, which indicates that part of the bulk carbon matrix converted to flake graphite carbon.[43] FAC$_3$ has large and folded graphite carbon layers with some pores, and HAC$_3$ has more graphite carbon fragments and pores. These unique structures are useful for forming a double-layer interface between electrode and electrolyte solution, which be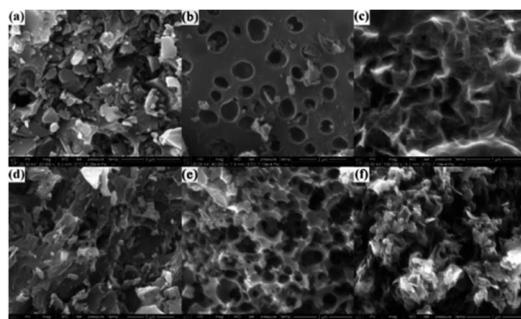nefit for the rapid diffusion of electrolyte ions from the surface into the interiors of FAC$_X$ and HAC$_X$ electrodes and reducing the resistance during the charge–discharge process.

The nitrogen adsorption and desorption isotherms of FAC$_X$ and HAC$_X$ are showed in Fig. 3a and c. It is obvious that the isotherm of FAC$_1$ belongs to the type-I, which means a typical microporous material, and the specific surface area of FAC$_1$ is 363.5 m^2 g^{-1}, the average pore diameter is 0.889 nm. When the activation temperature reached at 800 °C or 1000 °C, the isotherms of FAC$_2$ and FAC$_3$ change to the combination of type-I curve and type-IV curve, which show typical feature of micropores and meso-pores. It demonstrates that the two materials consist of both microporous structure and mesoporous structure,[44] the specific surface area of FAC$_2$ and FAC$_3$ are 1227.3 m^2 g^{-1} and 1501.6 m^2 g^{-1}, respectively, corresponding average pore size are 1.278 nm and 1.332 nm. However, HAC$_X$ materials all present the combined I/IV type isotherms, which are different from that of FAC$_X$. And the specific surface area of HAC$_1$, HAC$_2$ and HAC$_3$ are 957.2 m^2 g^{-1}, 1362.0 m^2 g^{-1} and 1667.5 m^2 g^{-1}, respectively, which are higher than that of FAC$_X$. Their corresponding average pore diameters are 1.030 nm, 1.186 nm and 1.352 nm, respectively. These materials, except FAC$_1$, possess interconnected hierarchical porous structure, which is beneficial to improving the supercapacitive performance. Studies have shown that micropores can offer a larger specific surface area to absorb electrolyte ions, mesopores can be used as rapid channels for ionic diffusion.[39]

The pore size distribution (shown in Fig. 3b and d) was obtained by DFT method. It is apparent that the pore size distributions of FAC$_1$ and HAC$_1$ are mainly focused on the range of microporous (below 2 nm), while FAC$_2$, FAC$_3$, HAC$_2$ and HAC$_3$ possess some small mesoporous, which are distributed at around 2–4 nm. In addition, the values of specific surface area and pore volume of FAC$_X$ and HAC$_X$ samples are showed in Table S1 (ESI†). According to these results, it can be seen that with the activation temperature increasing from 600 °C to 1000 °C, the BET area, micropore area, total pore volume and mesoporous number of FAC$_X$ and HAC$_X$ samples increase gradually, FAC$_3$ and HAC$_3$ possess the maximum specific

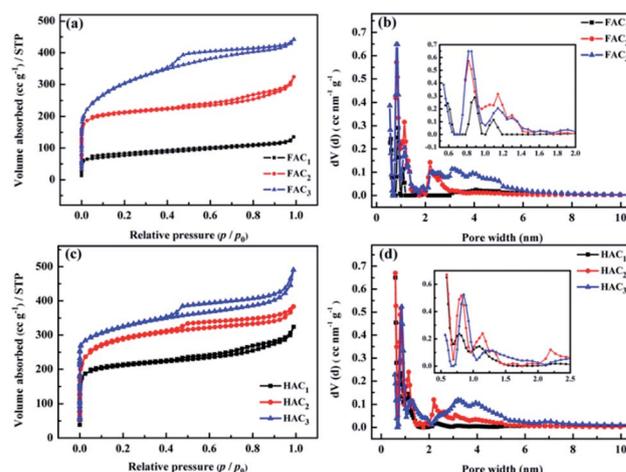Fig. 2 SEM images of (a) FAC$_1$, (b) FAC$_2$, (c) FAC$_3$, (d) HAC$_1$, (e) HAC$_2$ and (f) HAC$_3$.

Fig. 3 (a and c) N$_2$ adsorption–desorption isotherms and (b and d) pore size distributions of FAC$_X$ and HAC$_X$.

surface area of 1501.6 m^2 g^{-1} and 1667.5 m^2 g^{-1}, respectively. Though the average pore diameter of HAC$_2$ is smaller than that of FAC$_2$, the specific surface area and pore volume of HAC$_2$ are higher than that of FAC$_2$. The high specific surface area and suitable number of microporous and mesoporous have a crucial effect on supercapacitor energy storage.[45,46] The rich pore structure provides more active sites and electron transport channels for electrolyte ions, meanwhile improves the utilization rate of the active substance of the electrode. The hydrated cations such as K$^+$ and H$^+$ can easily get through these unique channels and contribute to energy storage because the sizes of bare and hydrated cations of electrolytes are smaller than 1 nm.[47] Therefore, it is predicted that the HAC$_2$ may exhibits better electrochemical capacitance than other samples because of the smaller pore size, the higher specific surface area and higher micropore volume as well as suitable mesopore.[32]

The crystal structures of FAC$_X$ and HAC$_X$ were further confirmed by XRD analysis and are displayed in Fig. 4a and b. It is obvious that the prepared carbon materials all present characteristic graphitic peaks located at around 24.7° and 43.7°, which can be ascribed to C (002) and C (101) plane reflection,[16,21,48,49] respectively. The high intensity in the low angle region indicates higher graphitization degree, which may be ascribed to the existence of the abundant micropores in all the samples,[49] is consistent with the N$_2$ sorption results. From Fig. 4a, the peaks of FAC$_2$ are very sharper, suggesting that it's crystalline and graphization degree improve. But the lower and enlarged width of peaks of FAC$_1$ and FAC$_3$ implies more amorphous nature of samples. In contrast with FAC$_X$, the C (002) peaks at around 24.7° of HAC$_X$ resemble each other in shape. However, the peak at 43° of HAC$_X$ is weakened gradually when the activation temperature became from 600 °C to 1000 °C, suggesting that the amorphous of HAC$_X$ increased with the increasing of activation temperature.

The graphitic structure of FAC$_X$ and HAC$_X$ was also characterized by Raman spectra (shown in Fig. 4c and d). Two featured peaks at around 1340 cm^{-1} (D-band) and 1600 cm^{-1} (G-band)

can be observed among all of these carbon materials, which are attributed to the defective carbon crystallites and the vibration of sp^2 carbon atoms,[50] respectively. It is interesting that FAC$_3$ and HAC$_3$ are detected second-order 2D peaks at around 2700 cm^{-1}. The 2D-band is sensitive to the number of graphene layers, indicating that the two materials possess a few well-graphitized layers. The relative intensity ratio of D-band to G-band (I_D/I_G) is extensively adopted to evaluate the graphitization degree of carbon materials; the lower I_D/I_G value signifies the higher graphitization degree of the materials.[51] It can be calculated that the I_D/I_G values of FAC$_1$, FAC$_2$ and FAC$_3$ are 0.87, 0.77 and 0.76, respectively, meanwhile I_D/I_G values of HAC$_1$, HAC$_2$ and HAC$_3$ are 0.90, 0.81 and 0.27, which indicate that the obtained carbon materials treated with higher activation temperature own better graphitization degree and lower crystal defects. The defect of hierarchical porous carbon can improve wettability, whereas carbon with the high graphitization degree can deliver a satisfying electrical conductivity and outstanding chemical stability. Hierarchical porous carbon with moderate I_D/I_G values may show high supercapacitive performance.

X-ray photoelectron spectroscopy (XPS) was carried out to analyze the main element and content of as-prepared FAC$_2$ (shown in Fig. 5a) and HAC$_2$ (shown in Fig. 5b). Three peaks concentrated at about 284.6, 401.0 and 533.2 eV are detected in the general spectroscopy, the values of these binding energy are corresponded to C 1s, N 1s and O 1s element, respectively. The fitting result of the spectrum indicates that FAC$_2$ mainly contains carbon (~88.38 at%) along with few amount of

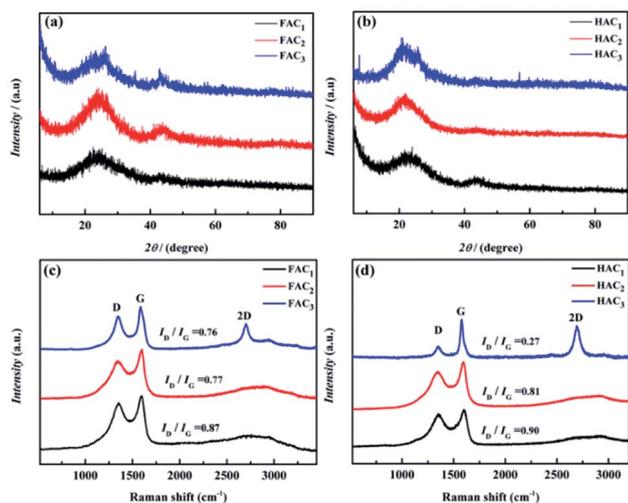Fig. 4 X-ray diffraction pattern of (a) FAC$_X$ and (b) HAC$_X$, and Raman spectroscopy of (c) FAC$_X$ and (d) HAC$_X$.
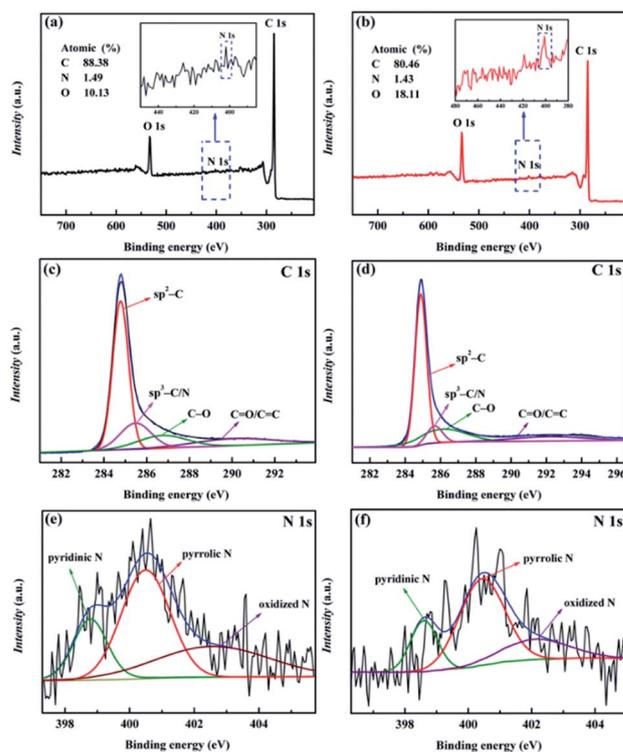

Fig. 5 XPS spectra of (a) FAC$_2$ and (b) HAC$_2$; (c) C 1s and (e) N 1s of FAC$_2$; (d) C 1s and (f) N 1s of HAC$_2$.

nitrogen (~1.49 at%) and oxygen (~10.13 at%), while the corresponding element content of HAC_2 are 80.46 at%, 1.43 at% and 18.11 at%, respectively, indicating that the N element content of HAC_2 is almost equal to that of FAC_2 and the O element content of HAC_2 is higher than that of FAC_2. Fig. 5c and d show the C 1s spectra of FAC_2 and HAC_2, respectively. Both of them are differentiated into four peaks, which include sp^2-C peak at 284.6 eV, sp^3-C/N peak at 285.6 eV, C–O peak at 286.6 eV and C=O/C=C peak at 289.8–291.8 eV, respectively. Furthermore, the N 1s spectra of FAC_2 and HAC_2 are shown in Fig. 5e and f, respectively, whose peaks located at 398.4, 400.3 and 402.7 eV can be assigned to pyridinic N (N-6), pyrrolic N (N-5) and oxidized N (N–X), which may be the decomposition product of organic ingredients. It is well known that oxygen and nitrogen functionalities could upgrade the surface wettability of carbon materials to facilitate the access of electrolyte and be involved in the faradaic reactions that enhance the pseudocapacitance of supercapacitor, which result in the better electrochemical performance.

Electrochemical performance characterization

The electrochemical properties of the prepared FAC_X and HAC_X electrodes were respectively investigated under a two-electrode configuration with 6.0 M KOH aqueous solution as electrolyte. The CV curves of FAC_X and HAC_X measured at a sweep rate of 50 mV s^{-1} are shown in Fig. 6a and 7a. In Fig. 6a, it is obvious that the CV profiles of FAC_2 electrode displays nearly rectangular, and the CV curve of FAC_2 exhibits great current response and displays the largest area among the FAC_X, indicating that FAC_2 possesses higher capacitance than FAC_1 and FAC_3. Moreover, there are no significant changes of rectangular characteristic of FAC_2 (shown in Fig. 6b) with the scan rate increasing from 5 mV s^{-1} to 50 mV s^{-1}. These indicate that FAC_2 demonstrates better electrical double layer capacitor (EDLC)

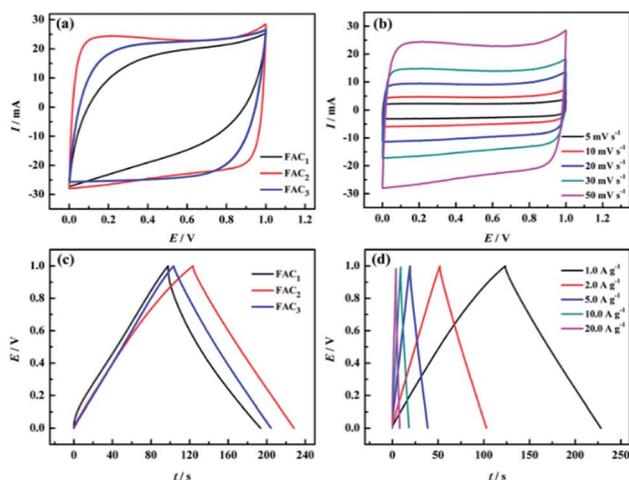**Fig. 6** Electrochemical performance of FAC_X measured in two-electrode system in 6.0 M KOH electrolyte. (a) CV curves of FAC_1, FAC_2 and FAC_3 at 50 mV s^{-1}; (b) CV curves of FAC_2 at different scan rates; (c) GCD curves of FAC_1, FAC_2 and FAC_3 at 1.0 A g^{-1}; (d) GCD curves of FAC_2 at different current densities.

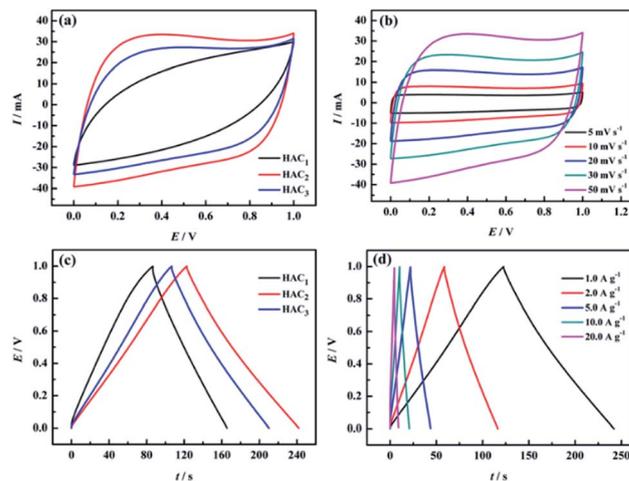**Fig. 7** Electrochemical performance of HAC_X measured in two-electrode system in 6.0 M KOH electrolyte. (a) CV curves of HAC_1, HAC_2 and HAC_3 at 50 mV s^{-1}; (b) CV curves of HAC_2 at different scan rates; (c) GCD curves of HAC_1, HAC_2 and HAC_3 at 1.0 A g^{-1}; (d) GCD curves of HAC_2 at different current densities.

behaviour and excellent electrochemical reversibility during the stage of charge–discharge.[52] By contrast, the shapes of CV curves of HAC_X (shown in Fig. 7a) measured at a sweep rate of 50 mV s^{-1} exhibit some similar and different characteristics from FAC_X, the CV profiles of HAC_2 and HAC_3 are quite similar to the rectangle profile of FAC_3 and are different from that of FAC_2, and HAC_2 also displays the largest area among the HAC_X materials. The elliptical shape of FAC_1 and HAC_1 indicates that they remain charge transfer resistance during the charge–discharge progress.[53] In addition, above results suggest that FAC_2 and HAC_2 fabricated at 800 °C exhibit better capacitance properties than those carbon materials fabricated at 600 °C or 1000 °C.

The galvanostatic charge–discharge (GCD) curves of FAC_X (shown in Fig. 6c) and HAC_X (shown in Fig. 7c) electrodes were measured at 1.0 A g^{-1}. All curves show an approximate isosceles triangle shape, which indicate excellent Coulomb efficiency and electrochemical reversibility at the stage of charge–discharge.[54] There are small voltage drops observed from GCD curves among of these electrode materials, indicating a low equivalent series resistance of FAC_X and HAC_X. It can be seen that the voltage drops of FAC_2 (shown in Fig. 6d) and HAC_2 (shown in Fig. 7d) continually rise along with the current density increase from 1.0 A g^{-1} to 20 A g^{-1}, which can be explained as follows: during the progress of charge–discharge the electrolyte ions will transport from the surface of electrode into the inner of electrode, at this time, the pore structure and pore size of electrode material make great influence on electrolyte ions, narrow pore diameter will greatly obstruct electrolyte ions to access to inner of electrode with the current intensity increase, thus result in larger voltage drops.[55] In addition, the GCD curves of FAC_2 and HAC_2 display longer discharge time than other prepared materials at 1.0 A g^{-1}, indicating that the two electrode materials exhibit higher specific capacitance, the corresponding specific capacitance of FAC_2 and HAC_2 calculated following
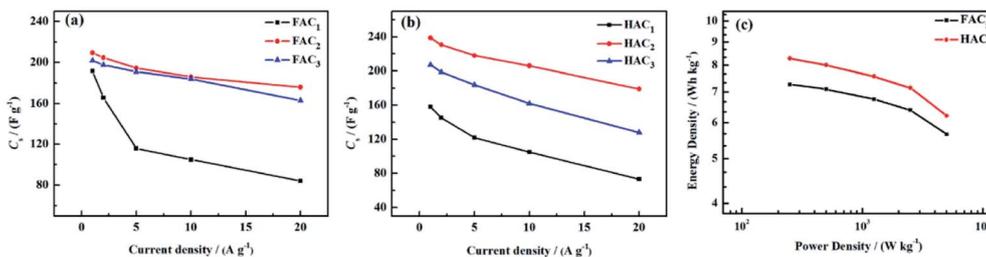
Fig. 8 Specific capacitance of (a) FAC_X and (b) HAC_X at different current densities; (c) Ragone plot of FAC_2 and HAC_2.

above formula (1) and (2) are 209.3 F g^{-1} and 238.6 F g^{-1}, respectively, which are higher than the values of commercial carbon materials (132 F g^{-1} at 0.2 A g^{-1})[24] and can be compared with some reported biomass carbon materials. The comparison of specific capacitance of some reported biomass-based carbon materials are listed in Table S2.†

Based on the discharge curves of those electrode materials, the specific capacitance values of FAC_X and HAC_X electrodes are also calculated following above formula (1) and (2), these results are given in Fig. 8a and b. The detailed data are shown in Table 1. Among FAC_X materials (shown in Fig. 8a) FAC_2 displays the highest specific capacitance and excellent rate performance, the specific capacitance of FAC_2 is 209.3, 204.6, 194.5, 186.0 and 176.0 F g^{-1} at current densities of 1.0, 2.0, 5.0, 10, 20 A g^{-1}, respectively. Its capacitance retention is 84.1% when the current density increases from 1.0 A g^{-1} to 20 A g^{-1}. And the specific capacitance values of FAC_3 are close to that of FAC_2 at the corresponding current densities, the specific capacitance of FAC_3 decrease from 201.8 F g^{-1} to 163.0 F g^{-1} with the capacitance retention of 80.8%. The specific capacitance of FAC_1 decays quickly with the increasing of current density. Compared with FAC_X, the highest specific capacitance value of HAC_2 electrode is 238.6 F g^{-1} at 1.0 A g^{-1}, higher than the specific capacitance of 158.3 F g^{-1} and 207.2 F g^{-1} of HAC_1 and HAC_3, respectively. Meanwhile the capacitance retention of HAC_1, HAC_2 and HAC_3 are 46.1%, 75.0% and 61.8% at 20 A g^{-1}. It is apparent that FAC_2 electrode shows the most excellent rate performance among FAC_X electrodes, and HAC_2 electrode displays more excellent rate performance than other prepared HAC_X electrodes. These results are ascribed to their unique O, N-codoped hierarchical pore structures of FAC_2 and HAC_2 materials, which have more reactive sites and conductive network providing more conductive channels and shortening the electrolyte ion transport path.[49] The specific

capacitance of HAC_2 electrode is higher than that of FAC_2 electrode, which is ascribed to the higher content of oxygen element for HAC_2. The more oxygen functional groups can offer extra pseudocapacitance. It is interesting that FAC_2 containing rich carbon element shows better rate performance than HAC_2. This may be the reason that the construction of HAC_2 possessing more defective carbon crystallites is easy to be destroyed under the high current density.

The energy density and power density are important parameters for evaluating the performance of supercapacitors. According to above formula (3) and (4), the energy density and power density values of FAC_2 and HAC_2 electrodes are calculated, and the Ragone plot is shown in Fig. 8c. It can be seen that the maximum energy densities of FAC_2 and HAC_2 are 7.3 W h kg^{-1} and 8.3 W h kg^{-1} with the same power density of ~250 W kg^{-1}, respectively, which are far higher than the value of commercial activated carbon based supercapacitors,[56] and it can be comparable with some reported biomass activated materials[24,26,31,35,45,57] and activated carbon[56] (listed in Table S3†). Moreover, even at a high power density of 5000 W kg^{-1} FAC_2 and HAC_2 still retain 5.7 W h kg^{-1} and 6.2 W h kg^{-1}, respectively, indicating excellent rate performance of the two electrodes.

Electrochemical impedance spectroscopy (EIS) is widely used to investigate the ion transport effect between electrolyte and electrode interface. The Nyquist plots of FAC_X and HAC_X are showed in Fig. 9a and b. The equivalent electrolyte ions transfer internal resistances at the electrode interface of FAC_1, FAC_2 and FAC_3 are almost 1.86 Ω, 0.94 Ω and 1.12 Ω in high frequency region, respectively, and the line of FAC_2 displays the straightest among that of FAC_X in the low frequency region, which indicates that FAC_2 electrode presents lower ion diffusion resistance and better capacitance behavior.[58] In contrast, the equivalent series resistances of HAC_1, HAC_2 and HAC_3 are 1.98 Ω, 0.62 Ω and 0.90 Ω, respectively, and HAC_2 electrode shows the

Table 1 Specific capacitance and rate performance of FAC_X and HAC_X electrodes at different current densities

| Sample	1.0 A g^{-1}	2.0 A g^{-1}	5.0 A g^{-1}	10.0 A g^{-1}	20.0 A g^{-1}	Capacitance retention
FAC_1	191.8 F g^{-1}	165.6 F g^{-1}	116.0 F g^{-1}	105.0 F g^{-1}	84.0 F g^{-1}	43.7%
FAC_2	209.3 F g^{-1}	204.6 F g^{-1}	194.5 F g^{-1}	186.0 F g^{-1}	176.0 F g^{-1}	84.1%
FAC_3	201.8 F g^{-1}	197.6 F g^{-1}	191.0 F g^{-1}	184.0 F g^{-1}	163.0 F g^{-1}	80.8%
HAC_1	158.3 F g^{-1}	145.4 F g^{-1}	122.0 F g^{-1}	105.0 F g^{-1}	73.0 F g^{-1}	46.1%
HAC_2	238.6 F g^{-1}	230.6 F g^{-1}	218.0 F g^{-1}	206.0 F g^{-1}	179.0 F g^{-1}	75.0%
HAC_3	207.2 F g^{-1}	198.8 F g^{-1}	184.0 F g^{-1}	162.0 F g^{-1}	128.0 F g^{-1}	61.8%
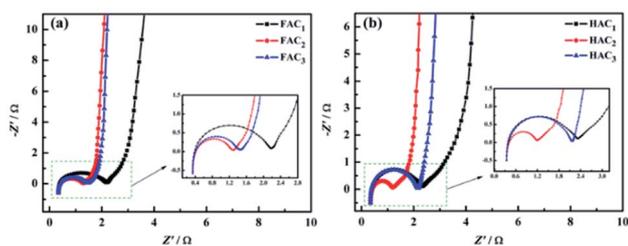
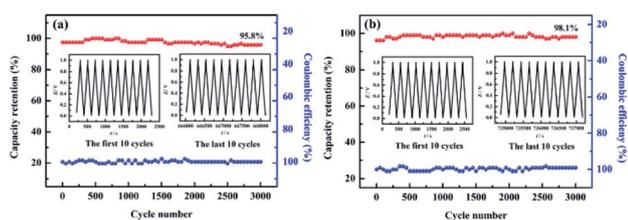**Fig. 9** Electrochemical impedance spectroscopy of (a) FAC_X and (b) HAC_X electrodes.

Fig. 10 Cycling stability and coulombic efficiency of (a) FAC_2 and (b) HAC_2 electrodes at 1.0 A g^{-1} for 3000 cycles. Inset: the GCD curves of the first and last ten cycles.

straightest line with a nearly 90° angle in the low frequency region, suggesting that it can efficiently reduce ions transfer resistance at the stage of charge–discharge and demonstrating ideal capacitance behavior. In essence, rich micro-mesoporous structure and high specific surface area of carbon materials can provide more efficient channels for electrolyte ions, which can shorten ion transport path, and greatly reduce charge transfer resistance and improve the utilization ratio of electrode active materials, and then improve the electrochemical performance.

The cycling lifetime for FAC_2 and HAC_2 materials were also investigated at the current density of 1.0 A g^{-1} in 6.0 M KOH. As shown in Fig. 10, FAC_2 and HAC_2 represent no apparent capacity shrinkage after 3000 cycles, and maintain 95.8% and 98.1% of the initial discharging capacity, respectively. Coulomb efficiency is also a mean of evaluating the electrochemical performance of supercapacitors, which is calculated by the ratio of discharge capacity to charge capacity during the same cycling process. The coulombic efficiency curves are showed in Fig. 10. It is apparent that the coulombic efficiency of FAC_2 (shown in Fig. 10a) and HAC_2 (shown in Fig. 10b) electrodes are around 100%, which indicate good reversible behavior and no any side reactions taking place during GCD cycling test.[59] In a word, the two electrode materials both present excellent cycling stability and outstanding charge–discharge efficiency.

Conclusions

FAC_X materials were prepared from black fungus and HAC_X materials were produced from *Hericium erinaceus via* KOH chemical activation. Different activation temperature has great effect on the pore structure and pore diameter of prepared carbon materials, and then influences their electrochemical

performance. The O, N-codoped FAC_2 and HAC_2 materials present unique hierarchical porous structure and satisfied surface area. Meanwhile FAC_X and HAC_X as electrode materials for supercapacitor exhibit an outstanding electrochemical performance, for instance, the satisfied specific capacitance of FAC_2 (209.3 F g^{-1}) and HAC_2 (238.6 F g^{-1}) at 1.0 A g^{-1}, excellent rate performance (the capacitance retention at 20 A g^{-1} of FAC_2 and HAC_2 are 84.1% and 75.0%, respectively) and prominent cycling performance (FAC_2 and HAC_2 almost no apparent capacity loss after 3000 cycles). And the corresponding maximum energy densities of FAC_2 and HAC_2 reach at 7.3 W h kg^{-1} and 8.3 W h kg^{-1}, respectively. These results imply that the oxygen-rich hierarchical porous carbon (HAC_2) shows higher specific capacitance and energy density and longer cycling performance. Nevertheless, carbon-rich hierarchical porous carbon (FAC_2) demonstrates excellent rate performance. The two biomass-derived porous and O, N-codoped activated carbons are potential electrode materials for supercapacitors.

Author contributions

Xinxian Zhong: data curation, formal analysis, writing original draft, funding acquisition. Quanyuan Mao: resources, formal analysis, visualization. Zesheng Li: formal analysis, visualization. Zhigao Wu: data curation, formal analysis. Yatao Xie: visualization. Shu-Hui Li: supervision, writing – review & editing. Guichao Liang: data curation, formal analysis. Hongqiang Wang: supervision, writing – review & editing, funding acquisition.

Conflicts of interest

There are no conflicts to declare.

Acknowledgements

Notes and references

1 H. D. Yoo, E. Markevich, G. Salitra, D. Sharon and D. Aurbach, *Mater. Today*, 2014, **17**, 110–121.
2 W.-L. Zhang, J. Yin, Z.-Q. Lin, J. Shi, C. Wang, D.-B. Liu, Y. Wang, J.-P. Bao and H.-B. Lin, *J. Power Sources*, 2017, **342**, 183–191.
3 Z. Bi, Q. Kong, Y. Cao, G. Sun, F. Su, X. Wei, X. Li, A. Ahmad, L. Xie and C.-M. Chen, *J. Mater. Chem. A*, 2019, 7, 16028–16045.
4 H. Zhao, L. Liu, R. Vellacheri and Y. Lei, *Adv. Sci.*, 2017, **4**, 1700188.
5 S. Cao, J. Yang, J. Li, K. Shi and X. Li, *Diamond Relat. Mater.*, 2019, **96**, 118–125.

6 Y. He, W. Chen, C. Gao, J. Zhou, X. Li and E. Xie, *Nanoscale*, 2013, **5**, 8799–8820.

7 C. Pan, Z. Liu, W. Li, Y. Zhuang, Q. Wang and S. Chen, *J. Phys. Chem. C*, 2019, **123**, 25549–25558.

8 Z. Zou and C. Jiang, *J. Alloys Compd.*, 2020, **815**, 152280.

9 J. Dominic, T. David, A. Vanaja, G. Muralidharan, N. Maheswari and K. K. S. Kumar, *Appl. Surf. Sci.*, 2018, **460**, 40–47.

10 V. Augustyn, P. Simon and B. Dunn, *Energy Environ. Sci.*, 2014, **7**, 1597–1614.

11 V. Ruiz, S. Roldán, I. Villar, C. Blanco and R. Santamaría, *Electrochim. Acta*, 2013, **95**, 225–229.

12 D. J. Kim, J. W. Yoon, C. S. Lee, Y.-S. Bae and J. H. Kim, *Appl. Surf. Sci.*, 2018, **439**, 833–838.

13 Z.-Q. Hao, J.-P. Cao, Y. Wu, X.-Y. Zhao, Q.-Q. Zhuang, X.-Y. Wang and X.-Y. Wei, *J. Power Sources*, 2017, **361**, 249–258.

14 L. Yao, Q. Wu, P. Zhang, J. Zhang, D. Wang, Y. Li, X. Ren, H. Mi, L. Deng and Z. Zheng, *Adv. Mater.*, 2018, **30**, 1706054.

15 J. Deng, M. Li and Y. Wang, *Green Chem.*, 2016, **18**, 4824–4854.

16 L. Miao, H. Duan, D. Zhu, Y. Lv, L. Gan, L. Li and M. Liu, *J. Mater. Chem. A*, 2021, **9**, 2714–2724.

17 Z. Song, L. Miao, L. Li, D. Zhu, L. Gan and M. Liu, *Carbon*, 2021, **180**, 135–145.

18 L. Miao, Z. Song, D. Zhu, L. Li, L. Gan and M. Liu, *Energy Fuels*, 2021, **35**, 8443–8455.

19 H. Peng, S. Qi, Q. Miao, R. Zhao, Y. Xu, G. Ma and Z. Lei, *J. Power Sources*, 2021, **482**, 228993.

20 Q. Ma, Y. Yu, M. Sindoro, A. G. Fane, R. Wang and H. Zhang, *Adv. Mater.*, 2017, **29**, 1605361.

21 X. Kang, H. Zhu, C. Wang, K. Sun and J. Yin, *J. Colloid Interface Sci.*, 2018, **509**, 369–383.

22 X.-L. Su, J.-R. Chen, G.-P. Zheng, J.-H. Yang, X.-X. Guan, P. Liu and X.-C. Zheng, *Appl. Surf. Sci.*, 2018, **436**, 327–336.

23 K. Wang, N. Zhao, S. Lei, R. Yan, X. Tian, J. Wang, Y. Song, D. Xu, Q. Guo and L. Liu, *Electrochim. Acta*, 2015, **166**, 1–11.

24 P. Cheng, S. Gao, P. Zang, X. Yang, Y. Bai, H. Xu, Z. Liu and Z. Lei, *Carbon*, 2015, **93**, 315–324.

25 R. Qiang, Z. Hu, Y. Yang, Z. Li, N. An, X. Ren, H. Hu and H. Wu, *Electrochim. Acta*, 2015, **167**, 303–310.

26 Y. Gong, D. Li, C. Luo, Q. Fu and C. Pan, *Green Chem.*, 2017, **19**, 4132–4140.

27 X. Hao, J. Wang, B. Ding, Y. Wang, Z. Chang, H. Dou and X. Zhang, *J. Power Sources*, 2017, **352**, 34–41.

28 X. Xu, J. Gao, Q. Tian, X. Zhai and Y. Liu, *Appl. Surf. Sci.*, 2017, **411**, 170–176.

29 Y.-Q. Zhao, M. Lu, P.-Y. Tao, Y.-J. Zhang, X.-T. Gong, Z. Yang, G.-Q. Zhang and H.-L. Li, *J. Power Sources*, 2016, **307**, 391–400.

30 M. S. Balathanigaimani, W.-G. Shim, M.-J. Lee, C. Kim, J.-W. Lee and H. Moon, *Electrochem. Commun.*, 2008, **10**, 868–871.

31 X. He, P. Ling, M. Yu, X. Wang, X. Zhang and M. Zheng, *Electrochim. Acta*, 2013, **105**, 635–641.

32 R. Zou, H. Quan, W. Wang, W. Gao, Y. Dong and D. Chen, *J. Environ. Chem. Eng.*, 2018, **6**, 258–265.

33 X. He, R. Li, J. Han, M. Yu and M. Wu, *Mater. Lett.*, 2013, **94**, 158–160.

34 X. Li, W. Xing, S. Zhuo, J. Zhou, F. Li, S.-Z. Qiao and G.-Q. Lu, *Bioresour. Technol.*, 2011, **102**, 1118–1123.

35 M. Xu, Q. Huang, J. Lu and J. Niu, *Ind. Crops Prod.*, 2021, **161**, 113215.

36 J. Li, L. Wei, Q. Jiang, C. Liu, L. Zhong and X. Wang, *Ind. Crops Prod.*, 2020, **154**, 112666.

37 D. Guo, L. Zhang, X. Song, L. Tan, H. Ma, J. Jiao, D. Zhu and F. Li, *New J. Chem.*, 2018, **42**, 8478–8484.

38 B. Liu, Y. Liu, H. Chen, M. Yang and H. Li, *J. Power Sources*, 2017, **341**, 309–317.

39 S. Sun, F. Han, X. Wu and Z. Fan, *Chin. Chem. Lett.*, 2020, **31**, 2235–2238.

40 N. F. Sylla, N. M. Ndiaye, B. D. Ngom, B. K. Mutuma, D. Momodu, M. Chaker and N. Manyala, *J. Colloid Interface Sci.*, 2020, **569**, 332–345.

41 Y. Wang, B. Ding, D. Guo and X. Wu, *Microporous Mesoporous Mater.*, 2019, **282**, 114–120.

42 H. Zhou, Y. Zhou, L. Li, Y. Li, X. Liu, P. Zhao and B. Gao, *ACS Sustainable Chem. Eng.*, 2019, **7**, 9281–9290.

43 A. Viinikanoja, J. Kauppila, P. Damlin, E. Mäkilä, J. Leiro, T. Ääritalo and J. Lukkari, *Carbon*, 2014, **68**, 195–209.

44 A.-Y. Lo, C.-T. Hung, N. Yu, C.-T. Kuo and S.-B. Liu, *Appl. Energy*, 2012, **100**, 66–74.

45 C. Gong, X. Wang, D. Ma, H. Chen, S. Zhang and Z. Liao, *Electrochim. Acta*, 2016, **220**, 331–339.

46 J.-P. Tessonnier, D. Rosenthal, T. W. Hansen, C. Hess, M. E. Schuster, R. Blume, F. Girgsdies, N. Pfänder, O. Timpe, D. S. Su and R. Schlögl, *Carbon*, 2009, **47**, 1779–1798.

47 C. Hun Yun, Y. Heum Park, G. Hwan Oh and C. Rae Park, *Carbon*, 2003, **41**, 2009–2012.

48 L. Qie, W.-M. Chen, Z.-H. Wang, Q.-G. Shao, X. Li, L.-X. Yuan, X.-L. Hu, W.-X. Zhang and Y.-H. Huang, *Adv. Mater.*, 2012, **24**, 2047–2050.

49 F. Sun, L. Wang, Y. Peng, J. Gao, X. Pi, Z. Qu, G. Zhao and Y. Qin, *Appl. Surf. Sci.*, 2018, **436**, 486–494.

50 M. Sevilla, C. Sanchís, T. Valdés-Solís, E. Morallón and A. B. Fuertes, *Carbon*, 2008, **46**, 931–939.

51 D. F. Li, G. Z. Yang, L. N. Qi, Q. B. Zheng and J. H. Yang, *Adv. Mater. Res.*, 2012, **487**, 860–863.

52 H. Guo, B. Ding, J. Wang, Y. Zhang, X. Hao, L. Wu, Y. An, H. Dou and X. Zhang, *Carbon*, 2018, **136**, 204–210.

53 H. Hwang, C. H. Kim, J.-H. Wee, J. H. Han and C.-M. Yang, *Appl. Surf. Sci.*, 2019, **489**, 708–716.

54 S. Ren, Y. Yang, M. Xu, H. Cai, C. Hao and X. Wang, *Colloids Surf., A*, 2014, **444**, 26–32.

55 S. Yoon, S. M. Oh, C. W. Lee and J. H. Ryu, *J. Electroanal. Chem.*, 2011, **650**, 187–195.

56 A. Burke, *Electrochim. Acta*, 2007, **53**, 1083–1091.

57 H.-h. Fu, L. Chen, H. Gao, X. Yu, J. Hou, G. Wang, F. Yu, H. Li, C. Fan, Y.-l. Shi and X. Guo, *Int. J. Hydrogen Energy*, 2020, **45**, 443–451.

58 M. Hou, K. Sun, X. Deng, F. Xiao and H. Yang, *RSC Adv.*, 2015, **5**, 74664–74670.

59 M. Li, J. P. Cheng, F. Liu and X. B. Zhang, *Electrochim. Acta*, 2015, **178**, 439–446.